Received: 9 April 2020 | Revised: 23 June 2020 | Accepted: 29 June 2020

DOI: 10.1002/ctpp.202000058

Contributions to Plasma Physics

ORIGINAL PAPER

Ion-acoustic solitary waves in e-p-i plasmas with (r, q)-distributed electrons and kappa-distributed positrons

Shahnaz Kouser[1] | **Muhammad Nouman Sarwar Qureshi**[1] | **Khalid Hussain Shah**[1] | **Hassan Amir Shah**[2]

[1]Department of Physics, GC University, Lahore, Pakistan

[2]Department of Physics, FCC (A Charted University), Lahore, Pakistan

Correspondence
Muhammad Nouman Sarwar Qureshi, Department of Physics, GC University, 54000 Lahore, Pakistan.
Email: nouman_sarwar@yahoo.com

Funding information
Higher Education Commission (HEC), Pakistan, Grant/Award Number: 7558/Punjab/NRPU/R&D/HEC/2017

Abstract

In this paper, we have studied the propagation of non-linear ion-acoustic waves in a plasma comprising of (r, q)-distributed electrons and kappa-distributed positrons. We have investigated the effect of complete electron distribution profile on the propagation of small, as well as arbitrary, amplitude solitons (via pseudopotential technique) by using generalized (r, q) distribution, which exhibits a spiky and flat top nature at low energies and a super-thermal tail at high energies. Interestingly, for negative values of r, solitons are formed with both polarities, positive (compressive) and negative (rarefactive), separately within a small amplitude limit and exist simultaneously in an arbitrary amplitude limit. We also found that the propagation of solitons has been affected by the change in parameters r, q, positron concentration, and electron to positron temperature ratio. The results presented in this study add to the fundamental understanding of the complete profile of the electron distribution function, high- and low-energy parts, and in the formation of compressive and rarefactive small and finite amplitude solitons in both space and astrophysical plasmas.

KEYWORDS

(r, q) distribution, e-p-i plasmas, ion-acoustic KdV solitons, kappa distributions, non-thermal distributions

1 | INTRODUCTION

The importance of electron-positron (e-p) plasmas has been realized in many natural space environments, such as the Milky Way, neutron stars, pulsar magnetosphere, and active galactic nuclei, as well as in intense laser field plasmas.[1–5] The presence of ions in astrophysical e-p plasmas and positron injection in usual electron-ion (e-i) laboratory plasmas would result in the formation of electron-positron-ion (e-p-i) plasmas.[6–8] The e-p-i plasmas have remained one of the most studied areas in the plasma physics community for the last couple of decades. Several studies have been devoted to non-linear electrostatic waves in e-p-i plasmas,[9–14] and it has been well established that wave propagation is considerably modified by the presence of positrons in e-i plasmas.[15–17]

Ion-acoustic solitary (IAS) waves have been the most studied plasma waves in collisionless e-i plasmas since the 60s, beginning with the seminal work of Washimi and Taniuiti[18], who derived the Korteweg-de Vries (KdV) equation for these waves. Later, a non-linear ion-acoustic (IA) wave was investigated in e-p-i plasmas, and it was found that the addition of positron as a third component in a plasma with singly charged ions and Boltzmannian electrons supressed the soliton

amplitude.[19] In another study, the effect of ion temperature has been investigated for arbitrary amplitude IAS waves, and it was found that soliton amplitude decreases, but there is an increase in upper Mach number with enhancement in ion temperature.[20] El-Awady et al.[21] studied IA waves in non-Maxwellian e-p-i plasmas, both in small and finite amplitude limits, in which kappa distribution was used to model both electrons and positrons. Several studies on non-Maxwellian plasmas have shown that wave characteristics change significantly due to the presence of non-thermal distributions and provided a better insight into the underlying physical processes.[22–26]

Kappa distribution has been used extensively to study various electrostatic and electromagnetic non-linear waves in astrophysical and space plasmas and is characterized by the spectral index κ, which basically models the particles with velocities greater than the thermal velocity. A smaller value of κ signifies a larger number of high-energy particles in the distribution and vice versa. In the large kappa limit, the kappa distribution tends to become Maxwellian distribution.[27] Vasyliunas[28] was the first who proposed kappa distribution to model the magnetospheric electrons. It has been observed that, for Earth's foreshock and planetary magnetospheres, it has values $3 < \kappa < 6$ [29], and in solar wind, its values lie between $2 < \kappa < 6$.[30–31] In addition to space plasmas, kappa distribution has also been observed in laboratory plasmas, such as in laser–matter interaction.[32] It has been shown that the presence of super-thermal particles predominantly modifies the IA shocks.[33] Studies on IA waves in arbitrary amplitude limit have shown that the solitary wave characteristics are modified due to the presence of non-thermal particles.[23–24,34–36]

In recent years, a more general distribution function has successfully been used to model the observed non-thermal particle distributions known as the generalized (r, q) distribution function.[25–26,37] In the last decade, Qureshi et al.,[38] in their pioneering work, empirically formulated this distribution function to fit the observed flat top in the particle velocity distribution profiles, which could not otherwise fit, by using other non-Maxwellian distribution functions. The (r, q) distribution not only gives flat tops but also models spikes at low energies along with the modelling of high-energy particles. The (r, q) distribution function is the generalizes of the Druyvesteyn–Davydov distribution $f \propto \exp[-(v^2/v_{th}^2)^r]$, the Maxwellian distribution $f \propto \exp[-(v^2/v_{th}^2)]$, and the power law kappa distribution $f \propto \left[1 + \frac{v^2}{\kappa^2 v_{th}^2}\right]^{-(\kappa+1)}$, and in the limiting cases $(r > 0, q \to \infty)$, $(r = 0, q \to \infty)$, and $(r = 0, q \to (\kappa + 1))$ reduces to Druyvesteyn–Davydov, Maxwellian, and kappa distributions, respectively. The (r, q) distribution has successfully been applied to interpret density humps and depletion non-linear structures while studying electrostatic solitary waves in a series of papers.[22,39] Saba et al.[23,36,40] studied linear and non-linear kinetic Alfven waves and their coupling with IA waves and successfully applied their results to interpret the observations of non-linear structures in space plasmas. In a simulation study, Khalilpour[41] modelled a hot electron beam with (r, q) distribution to simulate Langmuir waves in plasmas. As (r, q) distribution has been successfully used to model electron distributions from space plasmas and can mimic other distributions by altering the values of r and q, we will use this distribution in this paper, along with kappa distribution, to investigate the propagation characteristics of IAS structures in e-p-i plasmas. A more general study in which both electrons and positrons will be considered to be (r, q) distributed is out of the scope of this first basic study and is left for future investigation.

2 | MODEL EQUATIONS

The non-linear propagation of IAS waves has been considered in e-p-i plasma. The model comprises unmagnetized, collisionless e-p-i plasma in which electrons are modelled by (r, q) distribution and positrons by the kappa distribution function. The non-linear dynamics of IA waves in one dimension are considered by the following model equations:

$$\frac{\partial n_i}{\partial t} + \frac{\partial (n_i v_i)}{\partial x} = 0, \tag{1}$$

$$\frac{\partial v_i}{\partial t} + v_i \frac{\partial v_i}{\partial x} + \frac{\partial \Phi}{\partial x} = 0, \tag{2}$$

$$\frac{\partial^2 \Phi}{\partial x^2} - n_e + n_i + n_p = 0. \tag{3}$$

In the above set of Equations (1)–(3), v_i is the ion fluid velocity normalized by $v_s = \left(\frac{k_B T_e}{m_i}\right)^{\frac{1}{2}}$; T_e is the electron temperature, and k_B is the Boltzmann's constant; and n_e, n_i, and n_p are the electron, ion, and positron densities, respectively, normalized by the unperturbed electron density. The time t and space coordinate x are normalized by $\omega_p^{-1} = \left(\frac{m_i}{4\pi n_0 e^2}\right)^{\frac{1}{2}}$

and Debye length $\lambda_D = \sqrt{\frac{k_B T_e}{4\pi n_0 e^2}}$, respectively. The electrostatic potential Φ is normalized by $\frac{k_B T_e}{e}$, and the equilibrium condition is $n_{e0} = n_{p0} + n_{i0}$.

Electrons are assumed to follow the (r, q) distribution function for which the total electron density can be written as[22,36]

$$n_e = (1 + A_{rq}\,\Phi + B_{rq}\,\Phi^2), \tag{4}$$

where

$$A_{rq} = \frac{(q-1)^{-\frac{1}{(1+r)}}}{2\,C}\,\frac{\Gamma\left(\frac{1}{2(1+r)}\right)\,\Gamma\left(q-\frac{1}{2(1+r)}\right)}{\Gamma\left(\frac{3}{2(1+r)}\right)\,\Gamma\left(q-\frac{3}{2(1+r)}\right)}, \tag{5}$$

$$B_{rq} = \frac{3(q-1)^{-\frac{2}{(1+r)}}}{8\,C^2}\,\frac{\Gamma\left(1-\frac{1}{2(1+r)}\right)\,\Gamma\left(q+\frac{1}{2(1+r)}\right)}{\Gamma\left(1+\frac{3}{2(1+r)}\right)\,\Gamma\left(q-\frac{3}{2(1+r)}\right)}, \tag{6}$$

and

$$C = \frac{3\,(q-1)^{-1/(1+r)}\,\Gamma\left[q-\frac{3}{2+2\,r}\right]\Gamma\left[\frac{3}{2+2\,r}\right]}{2\,\Gamma\left[q-\frac{5}{2+2\,r}\right]\Gamma\left[\frac{5}{2+2\,r}\right]}. \tag{7}$$

We note that the spectral indices r and q follow the conditions $q > 1$ and $q(1+r) > 5/2$, [36–39] and constants A_{rq} and B_{rq} reduce to $A_{rq} = 1$ and $B_{rq} = 1/2$ and $A_{rq} = A_\kappa$ and $B_{rq} = B_\kappa$ for the Maxwellian and kappa values (given below), respectively.[24,36]

Kappa distribution is used to model the positrons[42], as follows

$$n_p = p\left(1 + \frac{\delta\,\Phi}{\left(\kappa - \frac{3}{2}\right)}\right)^{-\kappa+1/2}. \tag{8}$$

By expanding the above Equation (8) in the limit $\Phi \ll 1$, we obtain

$$n_p = p\,(1 - \delta\,A_\kappa\,\Phi + \delta^2\,B_\kappa\,\Phi^2), \tag{9}$$

where $\delta = \frac{T_e}{T_p}$, $p = \frac{n_{p0}}{n_{e0}}$, $A_\kappa = \frac{\left(\kappa-\frac{1}{2}\right)}{\left(\kappa-\frac{3}{2}\right)}$, $B_\kappa = \frac{\left(\kappa-\frac{1}{2}\right)\left(\kappa+\frac{1}{2}\right)}{2\left(\kappa-\frac{3}{2}\right)^2}$, and the limit on kappa is $\kappa > \frac{3}{2}$.

3 | SOLITARY SOLUTIONS

3.1 | Amplitude Limit

The KdV equation is derived by using the following stretched coordinates

$$\xi = \varepsilon^{\frac{1}{2}}(x - \lambda\,t)\text{and}\tau = \varepsilon^{\frac{3}{2}}t, \tag{10}$$

where λ is the linear phase velocity, and strength of non-linearity is measured by ε $(0 < \varepsilon < 1)$. The dependent quantities n_i, v, and Φ in perturbed form can be written as:

$$n_i = (1-p) + \varepsilon n_1 + \varepsilon^2 n_2 + \ldots, \tag{11}$$

$$v_i = v_0 + \varepsilon v_1 + \varepsilon^2 v_2 + \dots , \tag{12}$$

$$\Phi = \varepsilon\, \Phi_1 + \varepsilon^2\, \Phi_2 + \dots , \tag{13}$$

Upon using Equation (9) and the above perturbed quantities of Equations (10)–(12) in the set of Equations (1)–(3), by collecting terms in the lowest order in "ε", we get

$$n_1 = \frac{(1-p)v_1}{(\lambda - v_0)}, \tag{14}$$

$$v_1 = \frac{\Phi_1}{(\lambda - v_0)}, \tag{15}$$

$$\Phi_1 = \frac{n_1}{(A_{rq} + p\, A_\kappa\, \delta)}. \tag{16}$$

For the next order in ε, we obtain the following set of equations

$$\frac{\partial n_1}{\partial \tau} - (\lambda - v_0)\frac{\partial n_2}{\partial \xi} + (1-p)\frac{\partial v_2}{\partial \xi} + \frac{\partial (n_1 v_1)}{\partial \xi} = 0, \tag{17}$$

$$\frac{\partial v_1}{\partial \tau} - (\lambda - v_0)\frac{\partial v_2}{\partial \xi} + v_1 \frac{\partial v_1}{\partial \xi} + \frac{\partial \Phi_2}{\partial \xi} = 0\,, \tag{18}$$

$$\frac{\partial^2 \Phi_1}{\partial x^2} = (A_{rq} + p\, A_\kappa\, \delta)\Phi_2 - n_2 + (B_{rq} - p\, B_\kappa\, \delta^2){\Phi_1}^2. \tag{19}$$

We solve the above Equations (16)–(18) to eliminate second-order quantities in Φ and yield the following KdV equation in Φ_1:

$$\frac{\partial \Phi_1}{\partial \tau} + \alpha \frac{\partial {\Phi_1}^2}{\partial \xi} + \beta \frac{\partial^3 \Phi_1}{\partial \xi^3} = 0\,, \tag{20}$$

where $\alpha = \frac{1}{2}\left(\frac{3}{2(\lambda - v_0)} - \frac{(\lambda - v_0)^3}{(1-p)}(B_{rq} - p\, B_\kappa\, \delta^2)\right)$ is the non-linear coefficient, and $\beta = \frac{(\lambda - v_0)^3}{2(1-p)}$ is the dispersion coefficient. Upon introducing the new variable $\eta = (\xi - u\,\tau)$, where u is the velocity of the non-linear structure, we write the solution of KdV Equation (19) as

$$\Phi = \Phi_m Sech^2\left[\frac{\eta}{\Delta}\right]. \tag{21}$$

Here $\Delta = \sqrt{\frac{4\beta}{u}}$ is the width, and $\Phi_m = \frac{3u}{\alpha}$ is the amplitude of the soliton.

3.2 | Arbitrary amplitude solitary waves

In the previous section, we have applied the reductive perturbation technique and derived the KdV equation to study the ion-acoustic solitons. Solitary solution of the KdV equation gives us only small-amplitude non-linear structures, and we could not obtain arbitrary amplitude solitary structures, which can allow us to investigate other kinds of non-linear structures. Such fully non-linear structures have been studied in e-p-i and dusty plasmas.[43–47] Therefore, in this section, we study the arbitrary amplitude solitary waves and assume that all the dependent variables depend on a single variable $\eta = x - Mt$. Here, M is the Mach number, which is defined as the moving speed of the non-linear structure normalized by acoustic speed. By solving and integrating Equations (1) and (2) by using the boundary conditions $n_i \to (1-p)$, $n_p \to p$, $n_e \to 1$, $v_i \to 0$, and $\Phi \to 0$ when $\eta \to \pm\infty$, we can obtain the ion number density as follows:

$$n_i = \frac{(1-p)}{\sqrt{1 - \frac{2\Phi}{M^2}}}. \tag{22}$$

Upon using Equations (4), (9), and (21) in Equation (3), we can obtain

$$\frac{\partial^2\Phi}{\partial x^2} = (p-1) - (A_{rq} + p\,\delta\,A_\kappa)\Phi + (B_{rq} - p\,\delta^2\,B_\kappa)\Phi^2 + \frac{(1-p)}{\sqrt{1-\frac{2\Phi}{M^2}}} \equiv -\frac{\partial V(\Phi)}{\partial \Phi}. \tag{23}$$

The above equation is analogous to the particle in a one-dimensional potential well, where $V(\Phi)$ is the pseudopotential or Sagdeev potential. Integrating Equation (22) once using the same boundary conditions given above, the energy integral can be obtained as

$$\frac{1}{2}\left(\frac{d\Phi}{dx}\right)^2 + V(\Phi) = 0, \tag{24}$$

and the Sagdeev potential has the following form:

$$V(\Phi) = (p-1)\Phi - \frac{1}{2}(A_{rq} + p\,\delta\,A_\kappa)\Phi^2 - \frac{1}{3}(B_{rq} - p\,\delta^2\,B_\kappa)\Phi^3 + M^2(1-p)\left(1 - \sqrt{1-\frac{2\Phi}{M^2}}\right). \tag{25}$$

In order to obtain a soliton solution, Sagdeev potential Equation (25) must satisfy the following conditions:

$$V(\Phi)|_{\Phi=0} = 0 \quad V'(\Phi)|_{\Phi=0} = 0 \quad V''(\Phi)\big|_{\Phi=0} < 0$$

$$V(\Phi)|_{\Phi=\Phi_m} = 0 \qquad\qquad V'(\Phi)\big|_{\Phi=\Phi_m} > 0, \tag{26}$$

where Φ_m is the maximum value of potential. From the above Equation (26), Mach number M must fulfil the following condition to obtain a soliton solution from Equation (25).

$$M > \sqrt{\frac{1-p}{A_{rq} + p\,\delta\,A_\kappa}}. \tag{27}$$

4 | NUMERICAL RESULTS

Numerical analysis of the solitary wave solution (Equation (20)) for the KdV Equation (19) is presented in this section. We note that, in all the following figures, change in spectral indices r and q corresponds to the electron distribution, and a change in κ corresponds to positron distribution except in Figure 2, where we will consider kappa-distributed electrons to be the limiting case. Figure 1 depicts the hump soliton profiles for different values of $\kappa = 2, 3, 20$ for fixed values of $r = 1$, $q = 2$, except for the soliton shown in red, where $\kappa = 2$ and $r = 4$, $q = 2$, which corresponds to a flat top electron distribution as the flatness of the distribution increases when r increases. From Figure 1, we can see that the soliton becomes taller and wider with the increase in kappa index, that is, positrons tend to behave in a Maxwellian manner, and electrons exhibit a flat top nature. We can also note that the amplitude and width increase when the flat top nature of the electron distribution becomes more prominent, that is, spectral indices take the value $r = 4$, $q = 2$ even if the positrons exhibit a maximum high-energy tail, that is, when $\kappa = 2$.

Figure 2 shows the ion acoustic hump solitons when positrons are considered kappa distributed with a fixed $\kappa = 20$, and electrons are also considered to be kappa distributed with $\kappa = 2, 3, 20$, except the soliton in red where electrons are considered (r, q) distributed with $r = 4$, $q = 2$, which corresponds to a greater flat top electron distribution. It is evident from Figure 2 that a soliton becomes taller and its width becomes wider as the kappa increases when electrons follow the kappa distribution. However, when electrons are considered (r, q) distributed, both width and amplitude remain larger than the kappa case. Moreover, we only obtain compressive solitons for the cases of Maxwellian and kappa distributions.

Figure 3 depicts the maximum amplitude of hump solitons versus kappa index for different values of $r = 1, 2, 3, 4$, and $q = 2$. From Figure 3, we can see that the soliton's amplitude remains maximal for a larger value of r, which corresponds to a more flat top nature of the electron distribution. It is also evident from Figure 3 that the soliton becomes taller as kappa

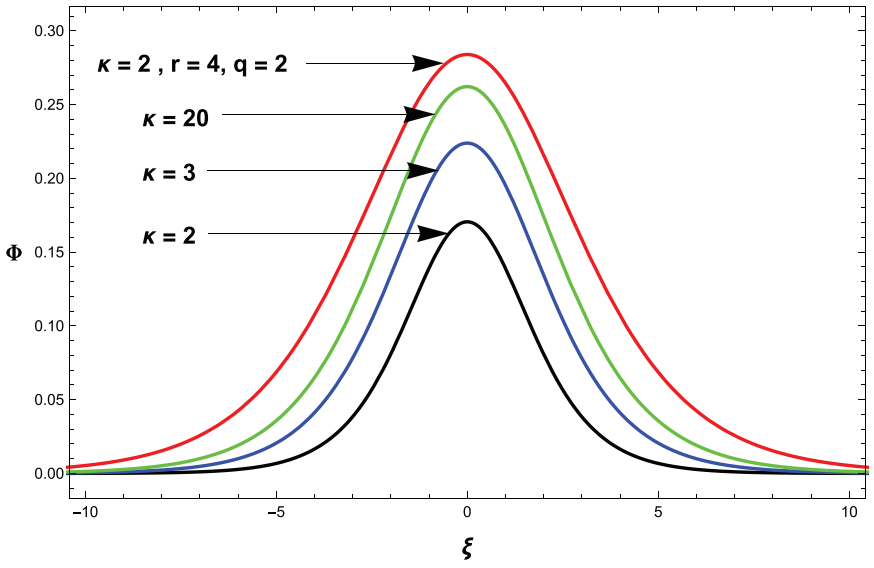

FIGURE 1 Ion-acoustic hump solitons when $r = 1$, $q = 2$ except for soliton in red, for which $r = 4$, $q = 2$ and different values of kappa $\kappa = 2$, 3, 20 and $\kappa = 2$. The other parameters are $u = 0.1$, $p = 0.4$, $\delta = 1$

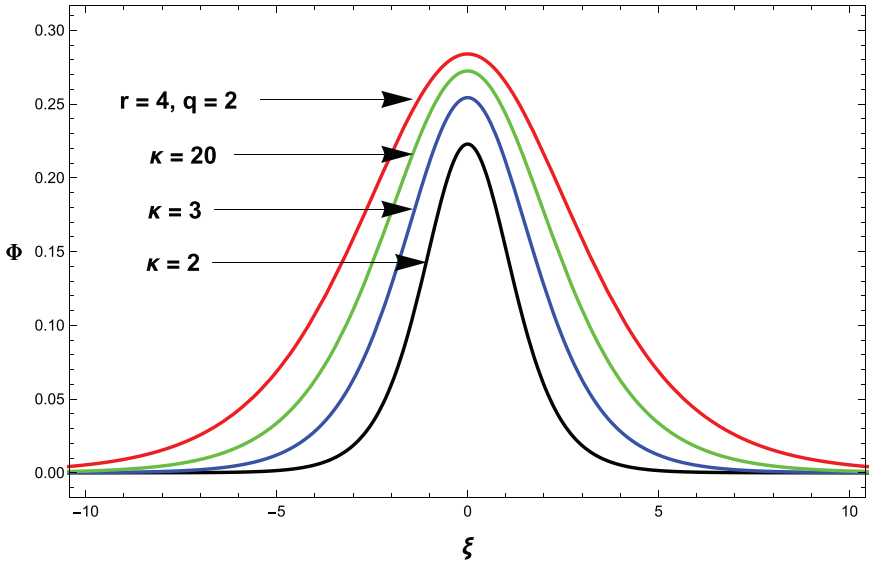

FIGURE 2 Ion-acoustic hump solitons when $\kappa = 2$ for positrons in all solitons and $\kappa = 2$, 3, 20 and $r = 4$, $q = 2$ for electron distribution. The other parameters are $u = 0.1$, $p = 0.4$, $\delta = 1$

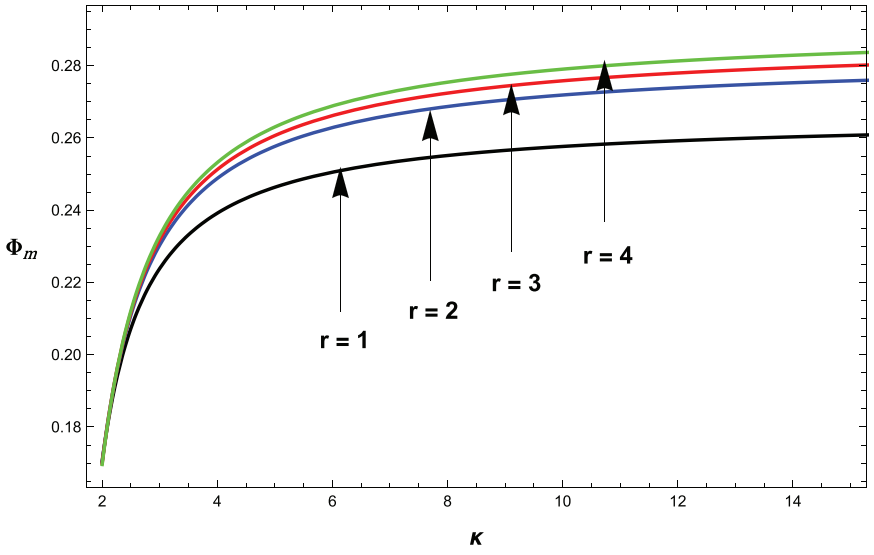

FIGURE 3 Maximum amplitude of compressive solitons versus kappa for different values of $r = 1$, 2, 3 and 4 when $q = 2$, $u = 0.1$, $p = 0.4$, $\delta = 1$

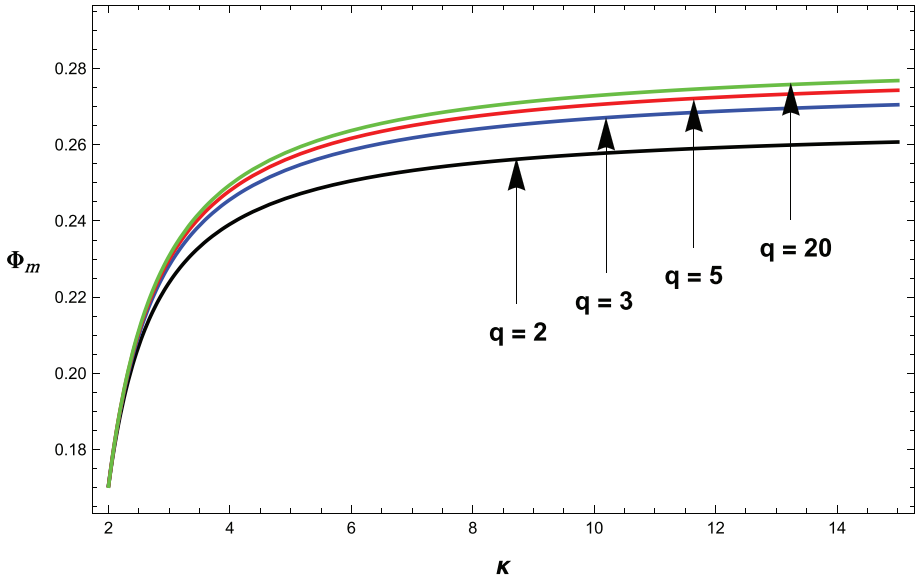

FIGURE 4 Maximum amplitude of compressive solitons versus kappa for different values of $q = 2, 3, 5$ and 20 when $r = 1$, $u = 0.1$, $p = 0.4$, $\delta = 1$

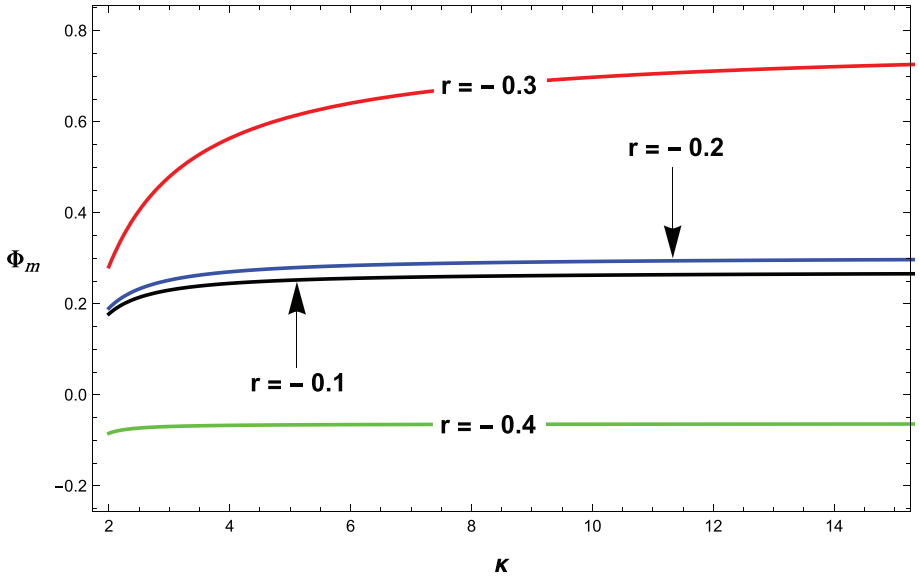

FIGURE 5 Maximum amplitude of compressive and rarefactive ion-acoustic solitons versus kappa for different negative values of $r = -0.1, -0.2, -0.3$ and -0.4 when $q = 5$, $u = 0.1$, $p = 0.4$, $\delta = 1$

increases, but the increase is much sharper for $2 < \kappa < 6$, after which the increase in amplitude levels off. Figure 4 depicts the maximum amplitude of the IA hump solitons versus kappa index for different values of $q = 2, 3, 5, 20$, and $r = 1$. From Figure 4, we can see that the soliton's amplitude remains maximum for larger values of q, which shows that electron distribution tends to behave in a Maxwellian way. It can also be seen from Figure 4 that the soliton becomes taller with the increase in kappa, but again, the increase is much sharper for $2 < \kappa < 6$, after which the increase in amplitude becomes almost constant. A comparison of Figures 3 and 4 shows that the change in maximum amplitude is less significant with the change in q than with the change in r.

Figure 5 depicts the maximum amplitude of solitons versus kappa for different negative values of $r = -0.1, -0.2, -0.3, -0.4$ and $q = 5$ and portrays a very interesting result that cannot be shown in Maxwellian- or kappa-distributed plasmas. From Figure 5, we can see that soliton switches its polarity from positive to negative when the negative value of r increases, that is, electron distribution has more of spiky nature. We can note that, for the fixed value of κ, the maximum amplitude of compressive soliton increases as the negative value of r increases, and then, its polarity changes when $-0.3 < r < -0.4$ for the particular value of $q = 5$; for other values of q, the soliton may change its polarity for different values of r, which is evident from the condition $q(1 + r) > 5/2$. Figure 6 depicts the maximum amplitude of the rarefactive solitons versus kappa index for different values of $q = 5, 7, 9, 11$ and $r = -0.4$. It is evident from Figure 6 that the maximum amplitude of rarefactive soliton increases when the value of q increases, that is, high-energy tail of the

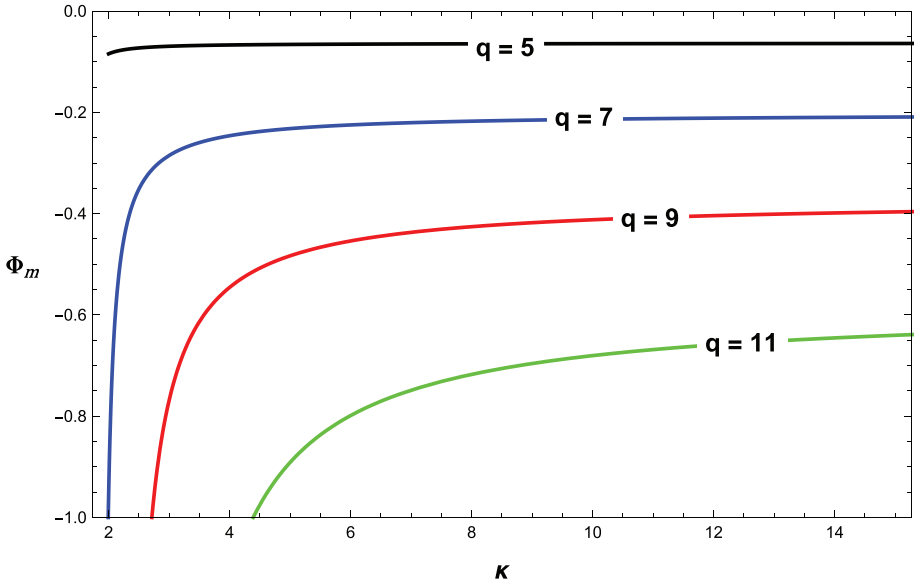

FIGURE 6 Maximum amplitude of rarefactive solitons versus kappa for different values of $q = 5, 7, 9$ and 11, when $r = -0.4$, $u = 0.1$, $p = 0.4$, $\delta = 1$

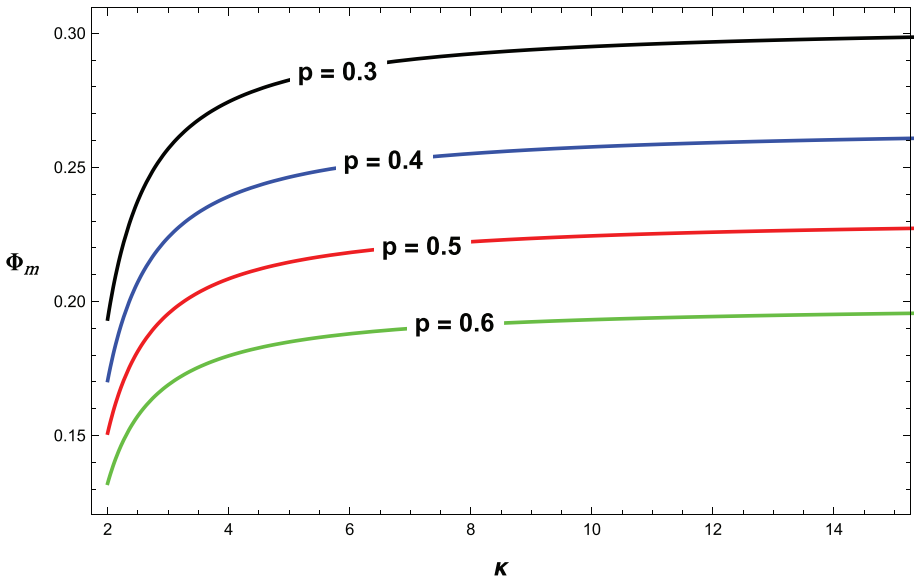

FIGURE 7 Maximum amplitude of compressive solitons versus kappa for different values of positron concentration $p = 0, 3, 0.4, 0.5, 0.6$ when $r = 1$, $q = 2$, $u = 0.1$, $\delta = 1$

electron distribution becomes less significant. We can see that the change in maximum amplitude of rarefactive soliton is more significant for larger values of q and for smaller values of κ.

Figure 7 depicts the maximum amplitude versus kappa index for different values of positron concentration $p = 0.3$, 0.4, 0.5, 0.6 when $r = 1$, $q = 2$. We can see that, for a fixed value of κ, the maximum amplitude of compressive solitons remains higher for the lower positron concentration. For the fixed value of positron concentration, maximum amplitude of compressive solitons increases with kappa, and this increase is significant for $2 < \kappa < 8$, after which an increase in amplitude becomes almost constant. Figure 8 shows the maximum amplitude of the rarefactive IA solitons versus kappa index for different values of positron concentration $p = 0.3$, 0.4, 0.5, 0.6 when $r = -0.4$, $q = 5$. We can see that, for the fixed value of κ, maximum amplitude of rarefactive solitons increases with the increase in positron concentration in contrast to Figure 7, where it increases with the decrease in concentration. We can also see that, for a fixed value of positron concentration, the maximum amplitude of compressive solitons decreases with an increase in kappa index, and this increase is significant for $2 < \kappa < 4$, after which the decrease in amplitude becomes almost constant.

Figure 9 depicts the maximum amplitude of the compressive ion-acoustic solitons versus kappa index for different values of electron to positron temperature ratio $\delta = 0.98$, 1.0, 1.02 when $r = 1$, $q = 2$ for electrons. We can see that, for the fixed value of κ, the maximum amplitude of compressive solitons increases with the increase in positron temperature. Moreover, for a fixed value of temperature ratio, the maximum amplitude of compressive solitons increases with the kappa

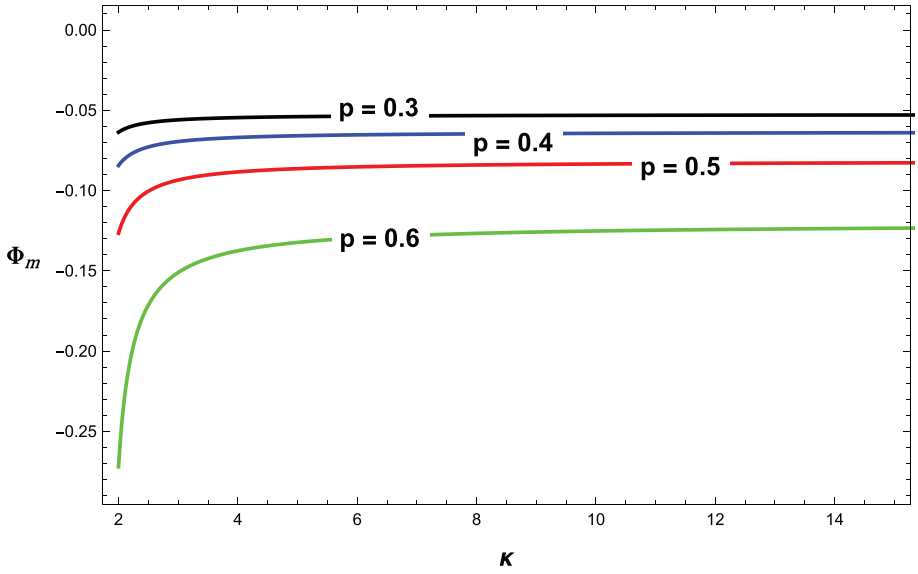

FIGURE 8 Maximum amplitude of rarefactive solitons for different values of positron concentration $p = 0$, 3, 0.4, 0.5, 0.6 when $r = -0.4$, $q = 5$, $u = 0.1$, $\delta = 1$

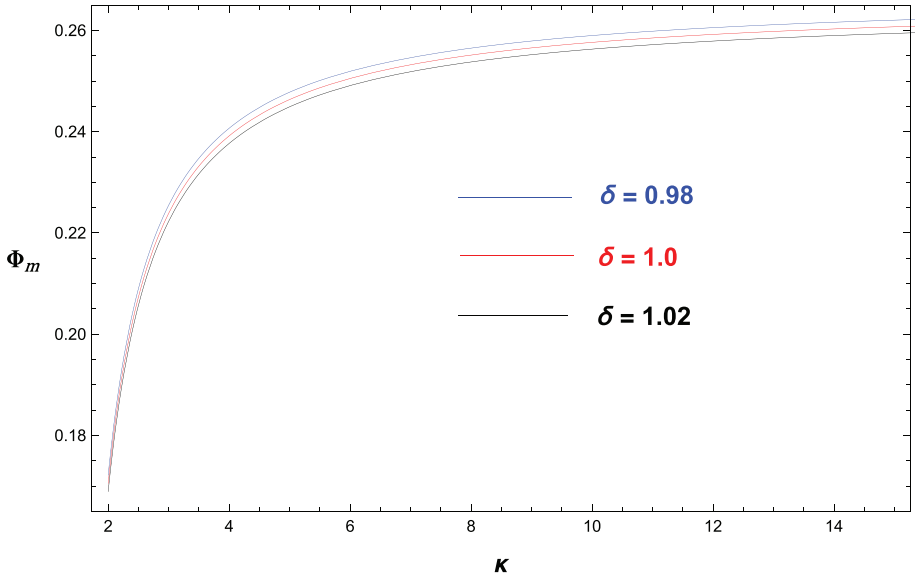

FIGURE 9 Maximum amplitude of compressive solitons versus kappa for different values of electron to positron temperature ratio $\delta = 0.98$, 1.0 and 1.02 when $p = 0.4$, $r = 1$, $q = 2$, $u = 0.1$

index, and this increase is significant for $2 < \kappa < 8$, after which the increase in amplitude becomes almost constant. We also investigated the effect of positron temperature on the maximum amplitude of rarefactive solitons for the negative value of r and found that, for the fixed value of κ, the maximum amplitude of rarefactive solitons increases with the decrease in positron temperature as shown in Figure 10, in contrast to the compressive solitons (Figure 9). We can also see that, for the fixed value of temperature ratio, the maximum amplitude of compressive solitons decreases when kappa increases.

Sagdeev potential and corresponding solitons are plotted in Figures 11–16, for which Equation (27) allows us to obtain subsonic and supersonic solitary structures. Figure 11 shows the Sagdeev potential and corresponding soliton structures for different values of $\kappa = 2$, 3, 7 when $M = 0.8$. We can see that solitons become taller, but their width decreases as κ decreases. Figure 12 shows the Sagdeev potential and corresponding soliton structures for different values of $\kappa = 2$, 3, 7 and for supersonic Mach number $M = 1.2$. We can see that solitons become taller, but their width decreases as κ increases in contrast to the subsonic case shown in Figure 11.

Figure 13 depicts the solitary structures for different values of Mach number ranging from subsonic to supersonic for the positive value of r. It can be seen that solitons become taller, and their width increases with the increase of Mach number from subsonic value to supersonic value. Figure 14 depicts the solitary structures of both polarity compressive and rarefactive simultaneously present for different values of subsonic Mach number and for negative value of r. It can

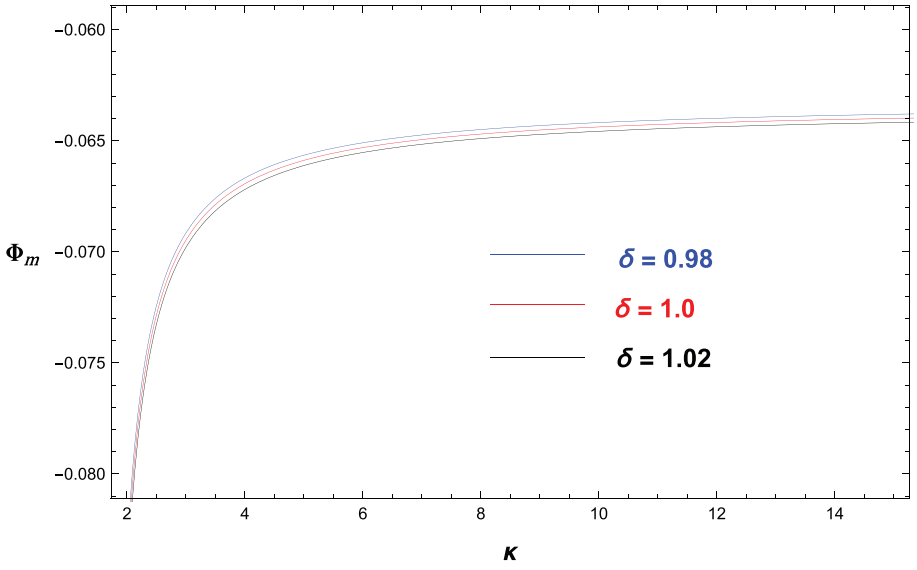

FIGURE 10 Maximum amplitude of rarefactive solitons versus kappa for different values of electron to positron temperature ratio $\delta = 0.98$, 1.0 and 1.02 when $p = 0.4$, $r = -0.4$, $q = 2$, $u = 0.1$

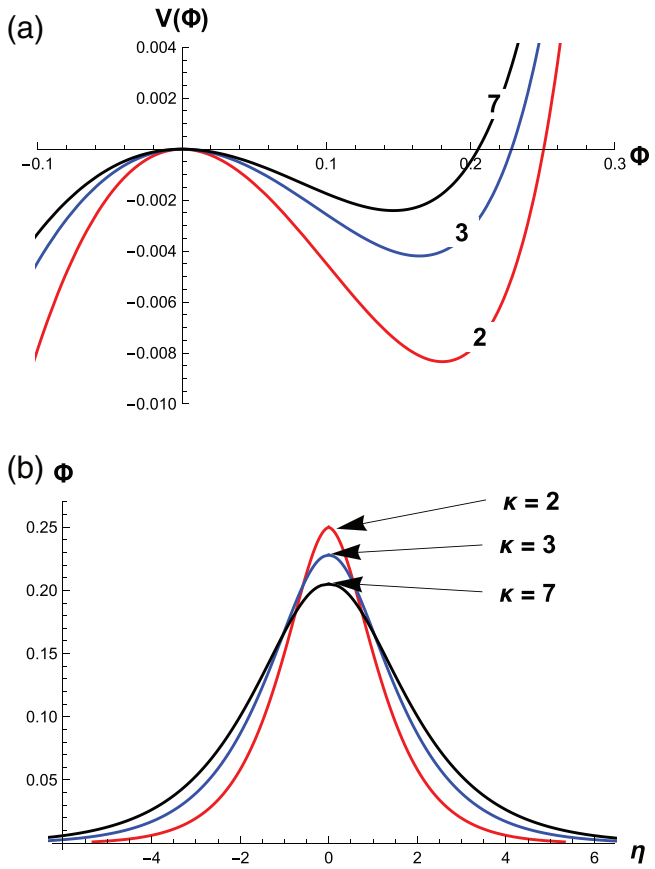

FIGURE 11 Sagdeev potential (a) and corresponding compressive solitons (b) for different values of kappa $\kappa = 2$, 3, and 7 when $M = 0.8$. The other parameters are $r = 1.0$, $q = 2$, $u = 0.1$, $\delta = 1$, $p = 0.4$

be seen that both compressive and rarefactive solitons become taller, but their width decreases with the increase of Mach number.

Figure 15 shows a very interesting result for different negative values of r in the subsonic regime. From Figure 15, we can see that as we increase the negative value of r, the soliton first shows a compressive nature and then both compressive and rarefactive behaviour simultaneously at a certain value of r and then switches its polarity to become rarefactive when negative r further increases. This behaviour could not be seen with a small amplitude limit. For compressive solitons, amplitude increases but width decreases as the negative values of r increases. For rarefactive solitons, amplitude and width both increase as negative values of r decrease. Figure 16 shows compressive solitary structures for different positive

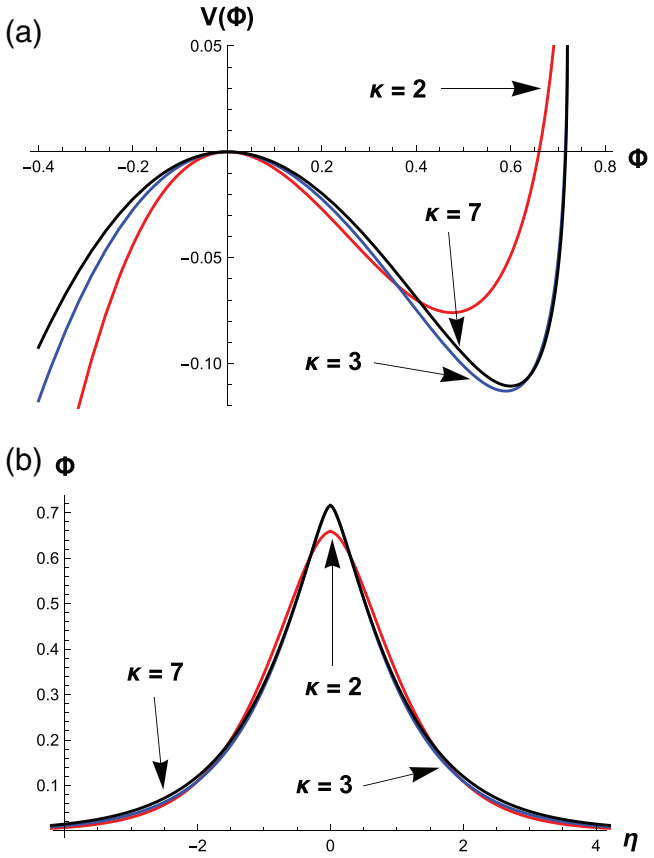

FIGURE 12 Sagdeev potential (a) and corresponding compressive solitons (b) for different values of kappa $\kappa = 2$, 3, and 7 when $M = 1.2$. The other parameters are $r = 1.0$, $q = 2$, $u = 0.1$, $\delta = 1$, $p = 0.4$

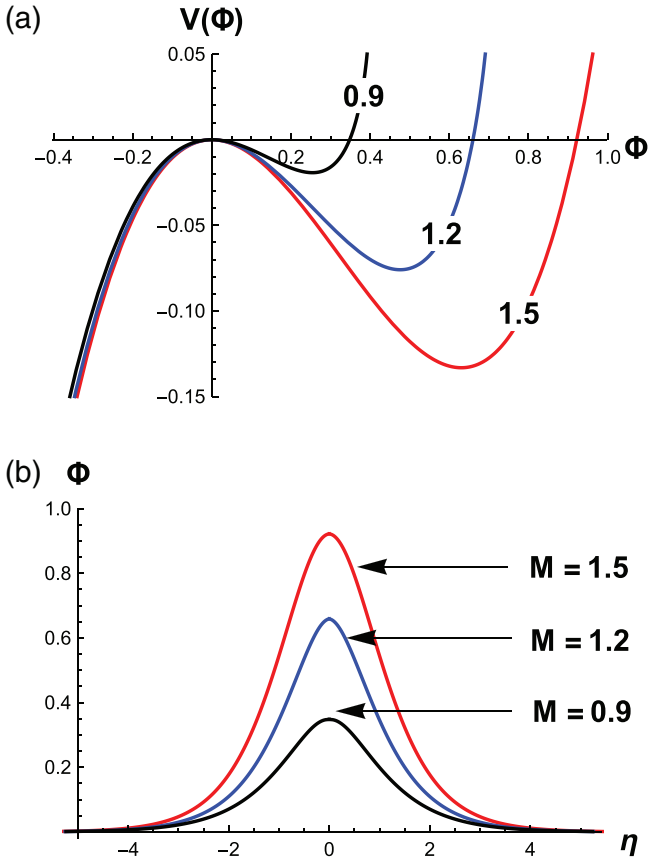

FIGURE 13 Sagdeev potential (a) and corresponding compressive solitons (b) for different values of Mach number $M = 0.9$, 1.2 and 1.5. The other parameters are $\kappa = 2$, $r = 1.0$, $q = 2$, $u = 0.1$, $\delta = 1$, $p = 0.4$

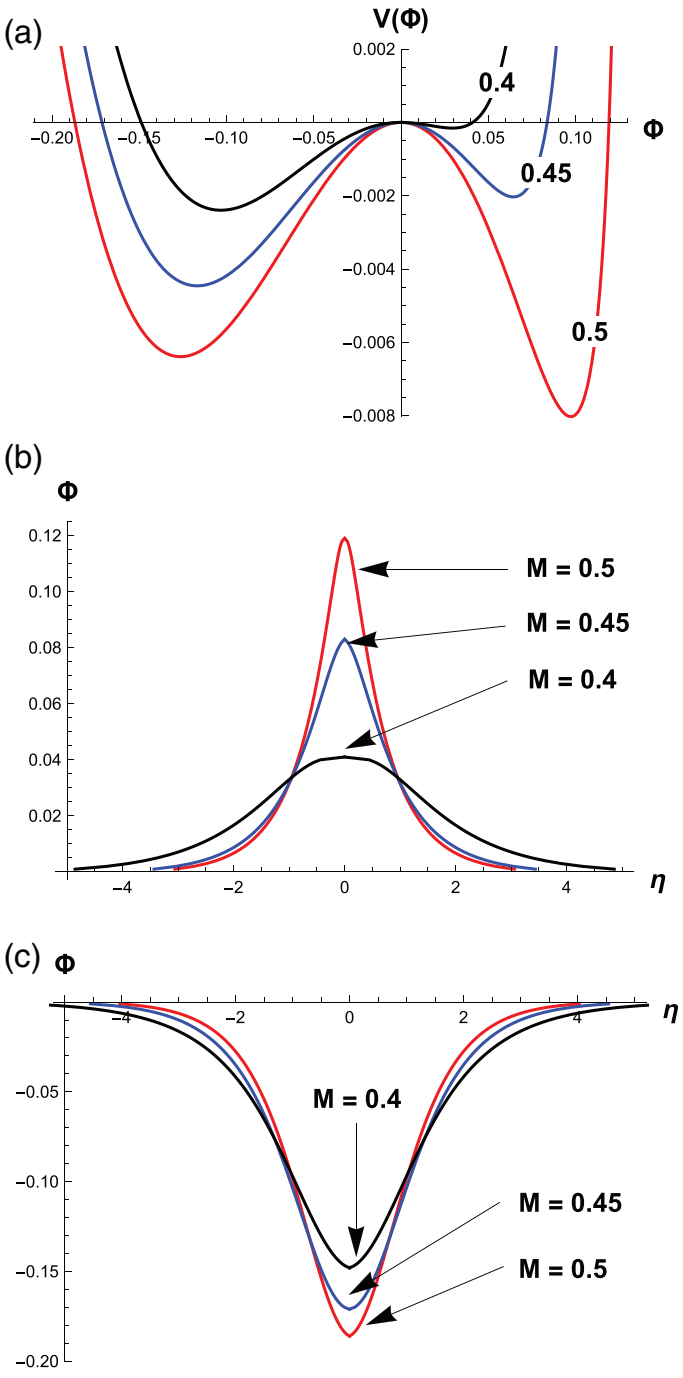

FIGURE 14 Sagdeev potential (a) and corresponding compressive (b) and rarefactive (c) solitons for different values of Mach number $M = 0.4, 0.45$ and 0.5 when $r = -0.3$. The other parameters are $\kappa = 2$, $q = 5$, $u = 0.1$, $\delta = 1$, $p = 0.4$

values of r in the supersonic regime. We note that solitons become taller, but their width decreases as r decreases. Figure 17 depicts the compressive solitary structures for positive r and different values of q in the supersonic regime. We can note that solitons become taller, but their width decreases as q decreases.

5 | SUMMARY AND CONCLUSION

For the first time, our investigations considered the non-linear propagation of IAS waves in a plasma comprising (r, q)-distributed electrons and kappa-distributed positrons to elucidate the importance and applicability of the complete distribution profile. Our investigation is based upon a generalized distribution for electrons, which could exhibit a spiky and flat top nature at low energies and super-thermal tails in the high-energy limit. We applied both the reductive perturbation

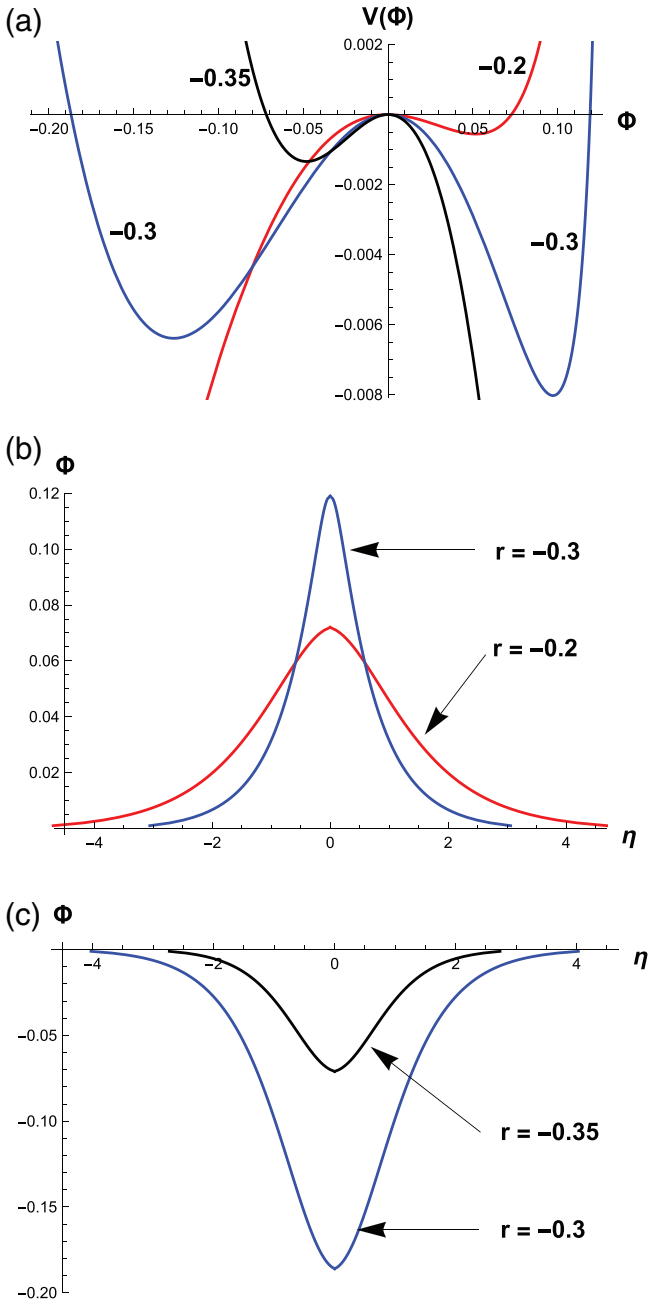

FIGURE 15 Sagdeev potential (a) and corresponding compressive (b) and rarefactive (c) solitons for different negative values of $r = -0.2, -0.3$, and -0.35 when $M = 0.5$. The other parameters are $\kappa = 2$, $q = 5$, $u = 0.1$, $\delta = 1$, $p = 0.4$

technique to derive the KdV equation and arbitrary amplitude pseudopotential technique to investigate the propagation characteristics of IAS waves based on the distribution profile by manipulating the values of spectral indices r and q. Our numerical results showed that the maximum amplitude of solitons turns out to be large for larger values of r and q for electron distribution, which correspond to the flat top nature of distribution, and remains minimum for kappa distribution. The interesting feature of the current study is the presence of solitons with both polarities, positive (compressive) and negative (rarefactive), for negative values of r, which could not be found in Maxwellian- and kappa-distributed plasmas. We found that compressive solitary wave amplitude increases as the negative value of r increases, and after a certain value, the polarity of the solitary wave reverses. For positive values of r, which correspond to flat top distribution, we only obtained compressive solitons whose amplitude increases with the increase in r. However, for negative values of r, which correspond to spiky distribution, both compressive and rarefactive solitons are obtained. Such spiky distributions have been observed in solar wind and Earth's magnetosphere.[48,49] Kiran et al.[50] successfully used (r, q) distribution with negative values of r to explain the adiabatic heating of solar wind, which could not be explained earlier when Maxwellian distribution was utilized. We also studied the effect of positron concentration on the amplitude characteristics of solitons.

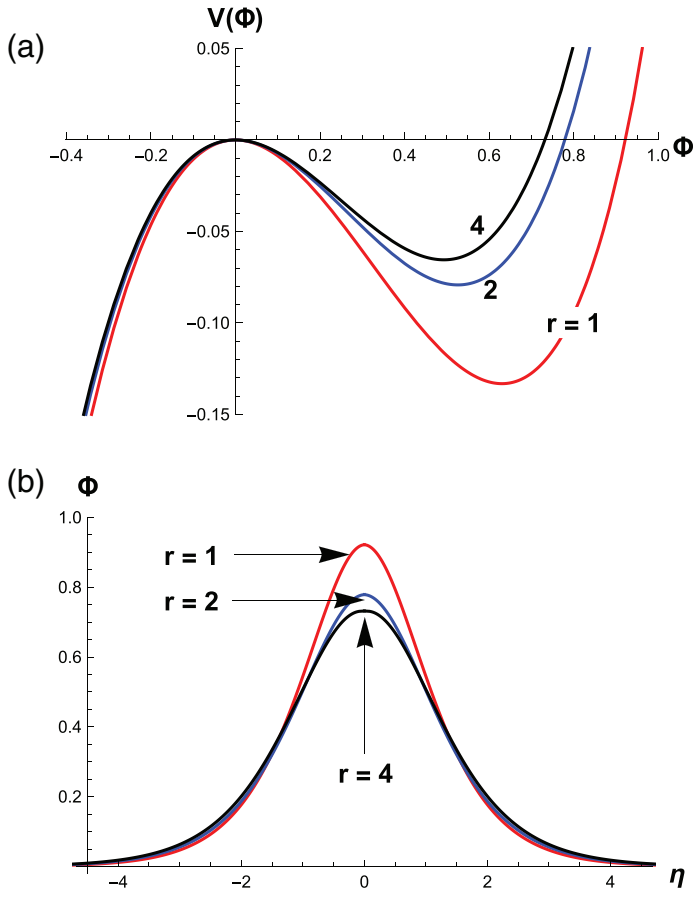

FIGURE 16 Sagdeev potential (a) and corresponding compressive (b) solitons for different positive values of $r = 1$, 2, and 4 when $M = 1.5$. The other parameters are $\kappa = 2$, $q = 2$, $u = 0.1$, $\delta = 1$, $p = 0.4$

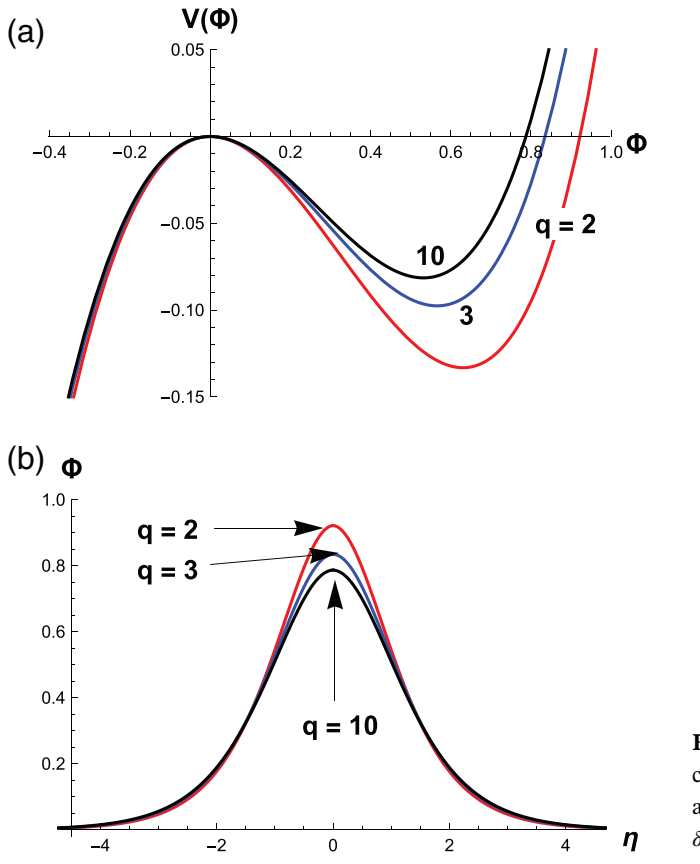

FIGURE 17 Sagdeev potential (a) and corresponding compressive (b) solitons for different positive values of $q = 2$, 3, and 10 when $M = 1.5$. The other parameters are $\kappa = 2$, $r = 1$, $u = 0.1$, $\delta = 1$, $p = 0.4$

Our results showed that the maximum amplitude of compressive solitons decreases, whereas the maximum amplitude of rarefactive solitons increases with the increase in positron concentration. The effect of the electron to positron temperature ratio has also been investigated, and we found that maximum amplitudes of compressive and rarefactive solitons increase with the decrease and increase in the temperature ratio, respectively, although the changes are not very large.

We also numerically solved the Sagdeev potential (25) and obtained the solitons by following the conditions (26) and (27). Our numerical results showed that solitons can be obtained for subsonic and supersonic regimes in kappa-distributed plasmas. In the subsonic regime, amplitude of the soliton increases, but in the supersonic regime, it decreases with the increase of super-thermal particles (i.e., $\kappa \to 3/2$). We also found that soliton amplitude increases with the increase in Mach number. In contrast to KdV solitons, amplitude of solitons corresponding to Sagdeev potentials decreases with flatness and when tails tends to be Maxwellian, that is, for large values of r and q. An interesting result of this study is the presence of compressive and rarefactive solitons simultaneously for a fixed value of negative r; the amplitude of such compressive and rarefactive structures increases with the increase in Mach number. Such a simultaneous presence of compressive and rarefactive solitons could not be found with a small amplitude limit. However, similar to KdV solitons, we found that the polarity of the soliton switches from compressive to rarefactive as we increase the negative value of r. The amplitude of compressive solitons increases, but the amplitude of rarefactive solitons decreases with the increase of negative value of r.

In conclusion, we would like to mention that the non-linear results presented in this paper are general, and the in situ observations of such non-linear waves in astrophysical plasmas are very difficult. However, the rapid development of laser technology, which includes chirped pulse amplification[51] and radiative blast waves,[52] would hopefully make it possible for us to compare the theory with experiments in future. Therefore, the results presented in this study elucidate the fundamental understanding of the complete profile of the electron distribution function, high- and low-energy parts, in the formation of compressive and rarefactive small and arbitrary amplitude solitons in both space and astrophysical plasmas.

ACKNOWLEDGMENT

This research was supported by the Higher Education Commission (HEC), Pakistan Project No. 7558/Punjab/NRPU/R&D/HEC/2017.

REFERENCES

[1] M. L. Burns, Positron-Electron Pairs in Astrophysics, American Institute of Physics, Melville, NY **1983**.
[2] F. C. Miller, P. J. Wiita, Active Galactic Nuclei, Springer, Berlin **1987**.
[3] F. C. Michel, *Rev. Mod. Phys.* **1982**, *54*, 869.
[4] F. C. Michel, Theory of Neutron Star Magnetosphere, Chicago University, Chicago, IL **1991**.
[5] V. Berezhiani, D. D. Tskhakaya, P. K. Shukla, *Phys. Rev. A* **1992**, *46*, 6608.
[6] T. Kotani, N. Kawai, M. Matsuoka, W. Brinkmann, *Publ. Astron. Soc. Jpn.* **1996**, *48*, 619.
[7] R. Greaves, C. Surko, *Phys. Rev. Lett.* **1995**, *75*, 3846.
[8] P. Helander, D. J. Ward, *Phys. Rev. Lett.* **2003**, *90*, 135004.
[9] S. Mahmood, A. Mushtaq, H. Saleem, *New J. Phys.* **2003**, *5*, 281.
[10] H. Saleem, S. Mahmood, *Phys. Plasmas* **2003**, *10*, 2612.
[11] H. Saleem, Q. Haque, J. Vranges, *Phys. Rev. E* **2003**, *67*, 057402.
[12] H. Saleem, *Phys. Plasmas* **2006**, *13*, 034503.
[13] R. Saeed, A. Shah, M. N. Ui Haq, *Phys. Plasmas* **2010**, *17*, 102301.
[14] S. Ali Shan, S. A. El-Tantawy, W. M. Moslem, *Phys. Plasmas* **2013**, *20*, 082104.
[15] A. P. Misra, A. R. Chowdhury, *Chaos, Solitons Fractals* **2003**, *15*, 801.
[16] R. G. Greaves, M. D. Tinkle, C. M. Surko, *Phys. Plasmas* **1994**, *1*, 1439.
[17] G. Sarri, W. Schumaker, A. Di Piazza, M. Vargas, B. Dromey, M. E. Dieckmann, V. Chvykov, A. Maksimchuk, V. Yanovsky, Z. He, *Phys. Rev. Lett.* **2013**, *110*, 255002.
[18] H. Washimi, T. Taniuiti, *Phys. Rev. Lett.* **1966**, *17*, 966.
[19] S. I. Popal, S. V. Vladimirov, P. K. Shukla, *Phys. Plasmas* **1995**, *2*, 716.
[20] Y. N. Nejoh, *Phys. Plasmas* **1996**, *3*, 1447.
[21] E. I. El-Awady, S. A. El-Tantawy, W. M. Moslem, P. K. Shukla, *Phys. Lett. A* **2010**, *374*, 3216.
[22] K. H. Shah, M. N. S. Qureshi, W. Masood, H. A. Shah, *Phys. Plasmas* **2018**, *25*, 042303.
[23] K. Saba, M. N. S. Qureshi, W. Masood, *Astrophys. Space Sci.* **2018**, *363*, 216.
[24] W. Massod, M. N. S. Qureshi, P. H. Yoon, H. A. Shah, *J. Geophys. Res.* **2015**, *120*, 101.
[25] M. N. S. Qureshi, K. H. Shah, J. Shi, W. Masood, H. A. Shah, *Contrib. Plasma Phys.* **2019**, *60*, e201900065.
[26] S. Sumbul, M. N. S. Qureshi, H. A. Shah, *AIP Adv.* **2019**, *9*, 025315.

[27] D. Summers, R. M. Thorne, *Phys. Fluids B* **1991**, *3*, 1835.
[28] V. M. Vasyliunas, *J. Geophys. Res.* **1968**, *73*, 2839.
[29] W. Feldman, S. Bame, S. Gary, J. Gosling, D. McComas, M. Thomsen, G. Paschmann, N. Sckopke, M. Hoppe, C. Russell, *Phys. Rev. Lett.* **1982**, *49*, 199.
[30] V. Pierrard, J. Lemaire, *J. Geophys. Res.* **1996**, *101*, 7923.
[31] M. Maksimovic, V. Pierrard, J. F. Lemaire, *Astron. Astrophys.* **1997**, *324*, 725.
[32] S. Magni, H. E. Roman, R. Bami, C. Riccardi, T. Pierre, D. Guyomarc'h, *Phys. Rev. E* **2005**, *72*, 026403.
[33] S. Sultana, I. Kourakis, N. S. Saini, M. A. Hellberg, *Phys. Plasmas* **2010**, *17*, 032310.
[34] S. Sultana, G. Sarri, I. Kourakis, *Phys. Plasmas* **2012**, *19*, 012310.
[35] A. Tahir, W. Masood, M. N. S. Qureshi, H. A. Shah, P. H. Yoon, *Phys. Plasmas* **2016**, *23*, 062307.
[36] K. Saba, M. N. S. Qureshi, W. Masood, *Phys. Plasmas* **2019**, *26*, 092114.
[37] M. N. S. Qureshi, W. Nasir, W. Masood, P. H. Yoon, H. A. Shah, S. J. Schwartz, *J. Geophys. Res.* **2014**, *119*, 10059.
[38] M. N. S. Qureshi, H. A. Shah, G. Murtaza, S. J. Schwartz, F. Mahmood, *Phys. Plasmas* **2004**, *11*, 3819.
[39] K. H. Shah, M. N. S. Qureshi, W. Masood, H. A. Shah, *AIP Advances* **2018**, *8*, 085010.
[40] K. Saba, M. N. S. Qureshi, W. Masood, *AIP Adv.* **2020**, *10*, 025002.
[41] H. Khalilpour, *Astrophys. Space Sci.* **2016**, *361*, 271.
[42] S. Asif, S. Mahmood, Q. Haque, *Phys. Plasmas* **2011**, *18*, 114501.
[43] G. Lu, Y. Liu, Y. Wang, L. Stenflo, S. I. Popel, M. Y. Yu, *J. Plasma Phys.* **2010**, *76*, 267.
[44] J. Srinivas, S. I. Popel, P. K. Shukla, *J. Plasma Phys.* **1996**, *55*, 209.
[45] T. V. Losseva, S. I. Popel, A. P. Golub, P. K. Shukla, *Phys. Plasmas* **2009**, *16*, 093704.
[46] T. V. Losseva, S. I. Popel, A. P. Golub, Y. N. Izvekova, P. K. Shukla, *Phys. Plasmas* **2011**, *19*, 013703.
[47] T. V. Losseva, S. I. Popel, A. P. Golub, *Plasma Phys. Rep.* **2012**, *38*, 729.
[48] M. N. S. Qureshi, G. Pallocchia, R. Bruno, M. B. Cattaneo, V. Formisano, H. Reme, M. J. Bosqued, I. Dandouras, J. A. Sauvard, L. M. Kistler, E. Mobius, B. Klecker, C. W. Carlson, J. P. McFadden, G. K. Parks, M. McCarthy, A. Korth, R. Lundin, A. Balogh, H. A. Shah, *Solar wind ten* **2003** Edited: M. Velli, R. Bruno, F. Malara.
[49] G. K. Parks, E. Lee, N. Lin, F. Mozer, M. Wilber, I. Dandouras, H. Reme, E. Lucek, A. Fazakerley, M. Goldstein, C. Gurgiolo, P. Canu, N. Cornilleau-Wehrlin, P. Decreau, *Phys. Rev. Lett.* **2007**, *98*, 265001.
[50] Z. Kiran, H. A. Shah, M. N. S. Qureshi, G. Murtaza, *Solar Phys.* **2006**, *236*, 167.
[51] D. Strickland, G. Mourou, *Opt. Commun.* **1985**, *56*, 219.
[52] R. A. Smith, *Bull. Am. Phys. Soc.* **2008**, *53*, 221.

How to cite this article: Kouser S, Qureshi MNS, Shah KH, Shah HA. Ion-acoustic solitary waves in e-p-i plasmas with (r, q)-distributed electrons and kappa-distributed positrons. *Contributions to Plasma Physics*. 2020;e202000058. https://doi.org/10.1002/ctpp.202000058